Theor Chem Acc (2003) 110:105–114
DOI 10.1007/s00214-003-0461-3

Theoretical
Chemistry Accounts

Regular article

Excited states of conjugated hydrocarbon radicals using the molecular mechanics – valence bond (MMVB) method

Michael J. Bearpark, Martial Boggio-Pasqua

Chemistry Department, King's College, Strand, London WC2R 2LS, UK

Received: 18 September 2002 / Accepted: 21 May 2003 / Published online: 15 August 2003

Abstract. By using a parameterised Heisenberg Hamiltonian coupled to a molecular mechanics force field, excited-state geometries were optimised for three conjugated hydrocarbon radicals: cyclopentadienyl, phenalenyl (perinaphthenyl), and triphenylmethyl. The results are compared with ab initio calculations, and with recent spectroscopic measurements.

Electronic Supplementary Material is available in the online version of this article at http://dx.doi.org/10.1007/s00214-003-0461-3

Keywords: Heisenberg Hamiltonian – Excited-state calculations – Valence bond theory – Conjugated hydrocarbon radicals – hybrid QM/MM methods

1 Introduction

In a recent perspective article [1] on the 1974 paper by Paldus [2] that introduced the unitary group approach into quantum chemistry, it was noted that this theory was becoming inaccessible to recently trained quantum chemists. The following reason was suggested: that once the insights described in Ref. [2] and related papers were obtained, code development and applications could proceed without the need to fully understand the mathematics (group theory) that led to these insights in the first place. Part of the purpose of this paper is to show that the graphical unitary group approach [3,4] devised by Shavitt [5,6] can be applied [7,8] in a simpler pictorial form to the valence bond (VB) method formulated as a Heisenberg Hamiltonian [9,10]. In doing this, we concentrate on the diagrams which both solved the problem originally and which were used subsequently to design the working computer code. Although there are many other codes for spin-only Hamiltonians [9, 22, 23, 24, 25, 26], and part of this work has been described previously [11], the pictorial method was not emphasised. When we reexamined the diagrams used in Ref. [11] recently and developed this presentation, we realised how they and our corresponding code could be modified to describe systems with an odd numbers of spins (as previously implemented in e.g. Ref. [9]), making the applications described later possible.

The matrix element code described here is included in the molecular mechanics – VB (MMVB) program [11,12]. Here, a parameterised Heisenberg Hamiltonian (describing an "active space" analogous to Complete-active-space self-consistent field, CASSCF) is coupled to an MM force field, making calculations on the ground and valence excited-states of large conjugated hydrocarbons possible. The results of excited-state geometry optimisations for three hydrocarbon radicals [13] are presented, as a test of MMVB with the modified matrix element code:

Cyclopentadienyl [14] (Five active electrons), a Jahn–Teller system which has been extensively studied experimentally.
Phenalenyl [15] (13 active electrons), recently crystallised in a spiro structure which is a neutral radical conductor [16].
Triphenylmethyl [17] (19 active electrons), the original hydrocarbon radical synthesised by Gomberg [18], whose photochemistry has recently been studied.

Our results are compared with CASSCF and time-dependent density functional theory (TDDFT) calculations where possible, and with recent spectroscopic studies.

2 Theory

The aim of this section is to show how VB matrix elements can be calculated pictorially, without explicitly using group theory [1]. We begin with a review in simpler language, based on Ref. [11]. We then describe how this approach was modified to describe systems with an odd numbers of spins.

Correspondence to: M.J. Bearpark
e-mail: michael.bearpark@kcl.ac.uk

The pictorial representation of the VB basis functions and matrix elements described later is based on but is far simpler than the one originally described by Shavitt [5,6], because in the VB case all orbitals are singly occupied, with either α or β spin. The VB Hamiltonian we are constructing is therefore a Heisenberg Hamiltonian. Although we are not using group theory explicitly, we use three key concepts derived from the group theoretical approach:

Representing many-electron basis functions graphically.
Associating a unique and predictable index with each basis function.
Using an integral-driven approach to compute nonzero offdiagonal matrix elements directly, without explicitly constructing the Hamiltonian matrix.

These three concepts are treated in turn later.

We start with Pascal's triangle (Fig. 1, top) [19], the arrangement in which each number at a particular horizontal level is the sum of the two numbers immediately above it. Notice that we have superposed Pascal's triangle over a grid: each number in the triangle is then the number of different ways of moving up from the corresponding point on the grid along the diagonals to the top, visiting each horizontal level only once.

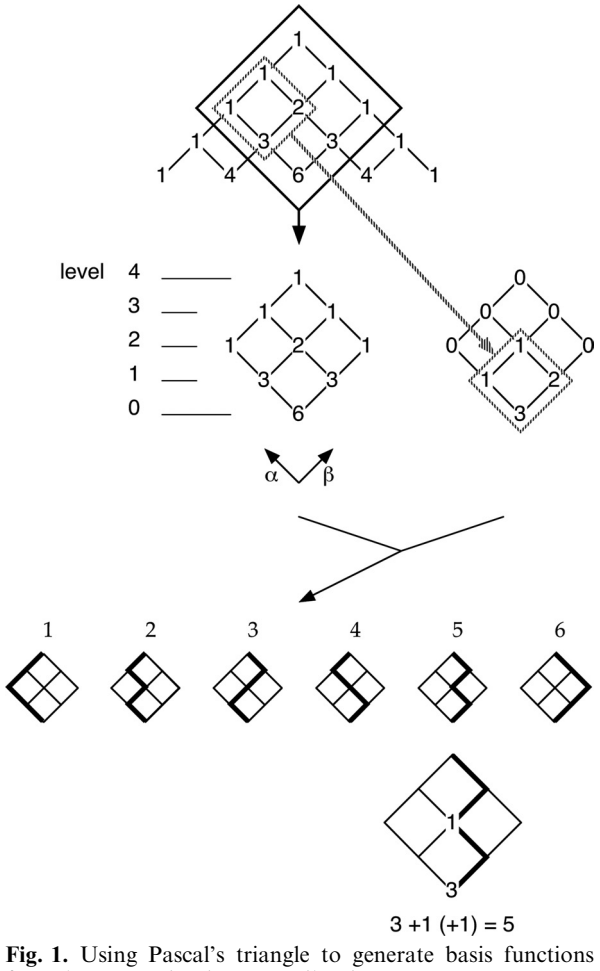

Fig. 1. Using Pascal's triangle to generate basis functions for a four-electron Heisenberg Hamiltonian

Fig. 1 (middle) shows that a subset of the Pascal's triangle grid can support the basis functions of a Heisenberg Hamiltonian: in this case, four singly occupied orbitals with either α or β electron spin. Starting at level zero, we add α and β electrons – two of each in this case – by moving in the up-left (α spin) and up-right (β spin) directions on the grid. For four electrons, the six resulting basis functions (actually Slater determinants) are shown at the bottom of Fig. 1. The first basis function shown is one for which orbitals 1 and 2 contain α electrons, and orbitals 3 and 4 contain β electrons. Each basis function has a total spin of zero; it is this restriction on the total spin that means we use the subset of Pascal's triangle shown.

The ordering of the basis functions at the bottom of Fig. 1 is intentional, because the sequence numbers shown can also be generated from a different grid based on Pascal's triangle, shown middle right. This grid contains offsets, which are added to the sequence number if a basis function moves in the up-right (β spin) direction from a particular point. Basis function 5 is shown as an example (Fig. 1, bottom): it moves in the up-right direction from levels 0 and 2; the corresponding offsets from the middle right grid are 3 and 1; the total offset is 4; and the final sequence number (starting at 1, not 0) is 5. The offset at any point on the grid is the total number of walks to the top which start in the up-left direction from that point. Equivalently, the offset is the total number of walks to the top from the point up-left of the present one, which explains why the particular subset of Pascal's triangle (shown by the hatched lines in Fig. 1) is used. It also explains why the offsets are only added to the sequence number when moving in the up-right direction.

So far, we have shown that the basis functions of the Heisenberg Hamiltonian can be represented graphically, and that a unique sequence number can be associated with each. Moreover, these unique sequence numbers are predictable (not random) because of the ordering described previously. The basis functions can therefore be generated "in sequence", and a particular basis function can be thought of as being "to the left of" or "to the right of" another on the grid (Fig. 1, bottom). This idea is central to the efficient evaluation of the offdiagonal matrix elements, described next.

The full Heisenberg Hamiltonian matrix for the four-electron problem introduced in Fig. 1 is shown in Fig. 2. The basis functions are in the same order 1 to 6, but written in a new notation, where $\underline{1}\ \underline{2}\ 3\ 4$ means that orbitals 1 and 2 contain α electrons, and orbitals 3 and 4 contain β electrons. The matrix elements shown in Fig. 2 were generated explicitly from Slater's rules. We concentrate on the off-diagonal matrix elements to start with. These occur when there are two spin-orbital differences between basis functions, and result in an integral indexed $K_{ij} = (ij|ij)$ (having the numerical value $[ij|ij] + 2 < i|h|j > S_{ij}$ for the VB problem [10]). For example, comparing basis functions 1 and 2, there is a difference between the spins of orbitals 2 and 3, leading to the integral $K_{32} = (32|32)$. There are also a number of zeros in off-diagonal positions, where the difference between basis functions is greater than two spin orbitals.

	1234	1234	1234	1234	1234	1234
1234	(1|1) (2|2) (3|3) (4|4) (22|11)-(21|21) (33|11) (33|22) (44|11) (44|22) (44|33)-(43|43)	(32|32)	-(42|42)	-(31|31)	(41|41)	0
1234	(32|32)	(1|1) (2|2) (3|3) (4|4) (22|11) (33|11)-(31|31) (33|22) (44|11) (44|22)-(42|42) (44|33)	(43|43)	(21|21)	0	(41|41)
1234	-(42|42)	(43|43)	(1|1) (2|2) (3|3) (4|4) (22|11) (33|11) (33|22)-(32|32) (44|11)-(41|41) (44|22) (44|33)	0	(21|21)	-(31|31)
1234	-(31|31)	(21|21)	0	(1|1) (2|2) (3|3) (4|4) (22|11) (33|11) (33|22)-(32|32) (44|11)-(41|41) (44|22) (44|33)	(43|43)	-(42|42)
1234	(41|41)	0	(21|21)	(43|43)	(1|1) (2|2) (3|3) (4|4) (22|11) (33|11)-(31|31) (33|22) (44|11) (44|22)-(42|42) (44|33)	(32|32)
1234	0	(41|41)	-(31|31)	-(42|42)	(32|32)	(1|1) (2|2) (3|3) (4|4) (22|11)-(21|21) (33|11) (33|22) (44|11) (44|22) (44|33)-(43|43)

Fig. 2. The full Heisenberg Hamiltonian matrix for the four-electron problem introduced in Fig. 1. Notation: underlining = α spin. $(ij|ij)$ indexes an integral having the numerical value $[ij|ij] + 2 < i|h|j > S_{ij}$ for the Valence bond (VB) problem [10]

The same Hamiltonian matrix as in Fig. 2 is shown in Fig. 3, but represented graphically by superimposing the walks from the bottom of Fig. 1. The nonzero offdiagonal matrix elements now appear as closed loops or boxes, which have been shaded in the figure. The matrix element K_{32} discussed earlier now appears as a box which opens from level 1 to level 2 (difference in electron 2 spin) and closes from level 2 to level 3 (difference in electron 3 spin). For spin orbitals which are the same, the corresponding walks either coincide — as for K_{32}, above and below the box — or move in parallel, to extend the box diagonally up-left and/or up-right. Zero offdiagonal matrix elements have been crossed out in Fig. 3: these correspond to differences of more than two spin orbitals between basis functions, and are represented by boxes which are either greater than one square wide on the grid, or which open and close more than once (both shown).

By itself, Fig. 3 does not lead to a more efficient algorithm for evaluating offdiagonal VB matrix elements. The current four-electron example hints at how this might be achieved, but to appreciate it, we have to imagine what happens as the number of electrons is increased.

In the four-electron example, there are a number of zero offdiagonal matrix elements (Figs. 2, 3). These increase in proportion rapidly as the number of electrons increases, so generating only the nonzero elements is advantageous. Fig. 2 shows that the matrix element K_{21} is generated between basis functions 4,2 and 5,3 but it is Fig. 3 which shows that these are both represented by the same box pattern. Moreover, because of the indexing scheme used, all of the possible shared walks from the top of this box run in sequence, and could be looped over. In general, a box will share many upper and/or lower walks, and there are few boxes relative to the number of pairs of basis functions that generate them. Hence a box(loop/shape/integral/K)-driven approach for generating offdiagonal matrix elements is very efficient: the box can be generated once, then all of the walks it shares can be looped over and the corresponding contributions to the Hamiltonian obtained.

Figure 4 shows that the nonzero offdiagonal matrix elements for the four-electron (n) problem (from Fig. 3) can actually be generated using walks from the two-electron ($n-2$) problem [11] as a guide. The two-electron walks are shown far left: each step in generating them is superposed on the four-electron problem towards the right, with a shaded square on the n grid around each point on an $n-2$ walk.

Figure 4 also shows that, once generated this way, K_{31} generates K_{32}, and K_{41} generates K_{42} and K_{43} by

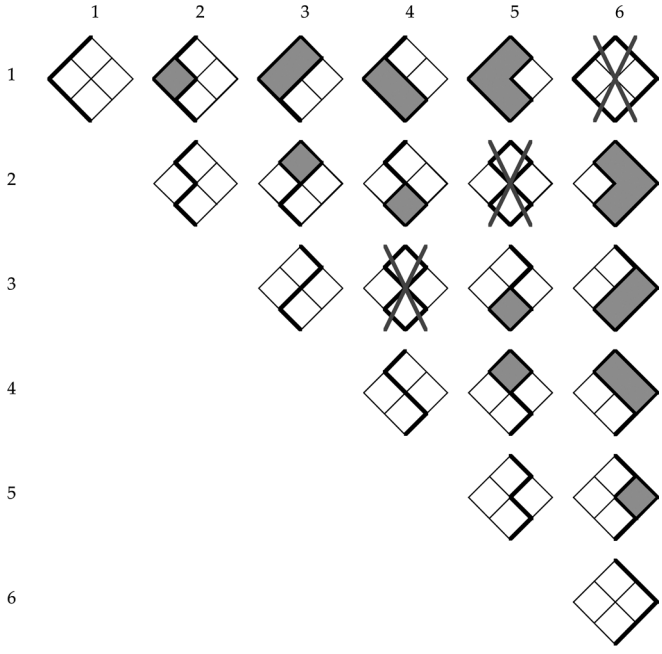

Fig. 3. The same Hamiltonian matrix as in Fig. 2, represented graphically by superimposing the walks from the bottom of Fig. 1. Off-diagonal exchange matrix elements K_{ij} – shown by shaded boxes – occur when there are two spin-orbital differences between basis functions

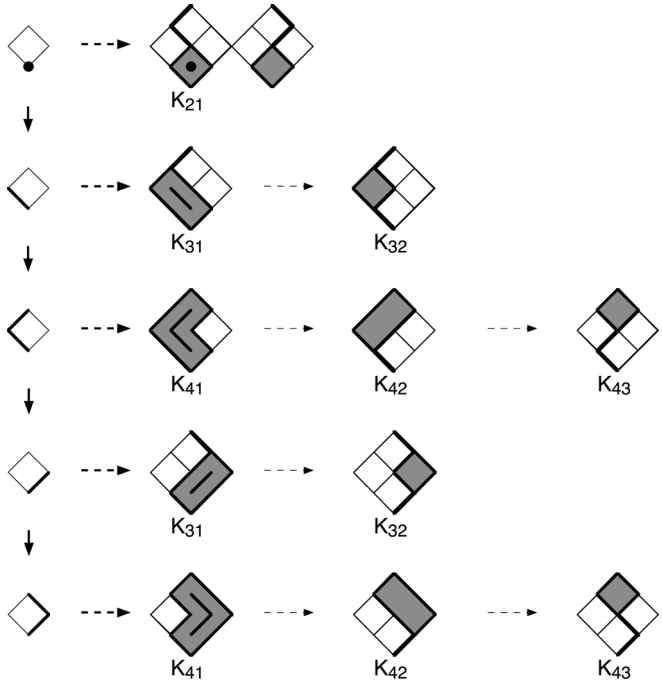

Fig. 4. The nonzero off-diagonal matrix elements shown as shaded boxes in Fig. 3 can be generated by following walks for a system with two fewer electrons

"collapsing" boxes to form a shared lower walk. All possible common upper walks are determined for each box/K_{ij}, as shown for K_{21}. There are two caveats. Firstly, Fig. 4 shows that the matrix element K_{32} between basis functions 1,2 and 5,6 corresponds to two distinct boxes, which are generated independently. Secondly, although the two occurences of K_{43} in Fig. 4 are represented by the same box, they are also generated independently at the present time: the algorithm currently generates all common upper walks (e.g. for K_{21}) but generates lower n walks from the $n-2$ walk which led to this point.

One feature missing from the discussion of the four-electron problem so far is symmetry. The grid generated from Pascal's triangle in Fig. 1 is symmetric about the vertical axis, and the pairs of basis functions at the bottom of Fig. 1 (1–6, 2–5, 3–4) are mirror images of each other. By working with only one of these pairs explicitly and treating the other implicitly [20], considerable savings can be made for larger problems, and in fact our original VB matrix element code [11] never constructed the full Slater basis. The reason for not emphasising symmetry here is that the full Slater basis must be constructed for the odd-electron problems discussed later, and the symmetry just described is broken.

However, having broken this symmetry, and by using the grid representation described earlier, the extension of our VB matrix element code to odd numbers of electrons is straightforward. The sections of Pascal's triangle necessary to generate the grids for the five-electron problem are shown in Fig. 5. We now have one more α electron than β electron, but otherwise the grids are generated in exactly the same way. The resulting ten walks (basis functions) are shown at the bottom of Fig. 5, and the corresponding matrix elements in the supplementary material.

In summary, the method reviewed for generating the matrix elements of an n-electron Heisenberg Hamiltonian consists of three steps:

1. Generate n and $n-2$ grids from Pascal's triangle.
2. Generate all possible basis functions (walks) from the n grid. The diagonal matrix elements K_{ij} are then generated from permutations within the α and β spins for each basis function.
3. Generate all possible walks for the $n-2$ problem. This gives offdiagonal matrix elements K_{ij} for the n problem.

3 Computational methods

The matrix element code described here has been used in two ways, depending on how the numerical values of Q_{ij} and K_{ij} for the Heisenberg Hamiltonian were determined.

Firstly, for testing, we used a standalone version of the code that reads in the K_{ij} between individual spin sites. We initially used "Huckel-like" parameters [21] describing connectivity, with $K_{ij} = 1.0$ between adjacent spin sites. There are several other implementations of this type of code [22,23,24,25,26].

The Lanczos diagonalisation method – iterative improvement of a guess for the lowest few eigenvectors – is used to avoid storing the full Hamiltonian matrix. The results were checked against full diagonalisation up to 13 spins (1716 determinant basis functions) to confirm that roots were not being missed. The starting guess for the Lanczos diagonalisation is determined by the largest diagonal contributions, with a small even or odd number chosen, depending on whether the number of electrons and the total number of basis functions generated is even or odd.

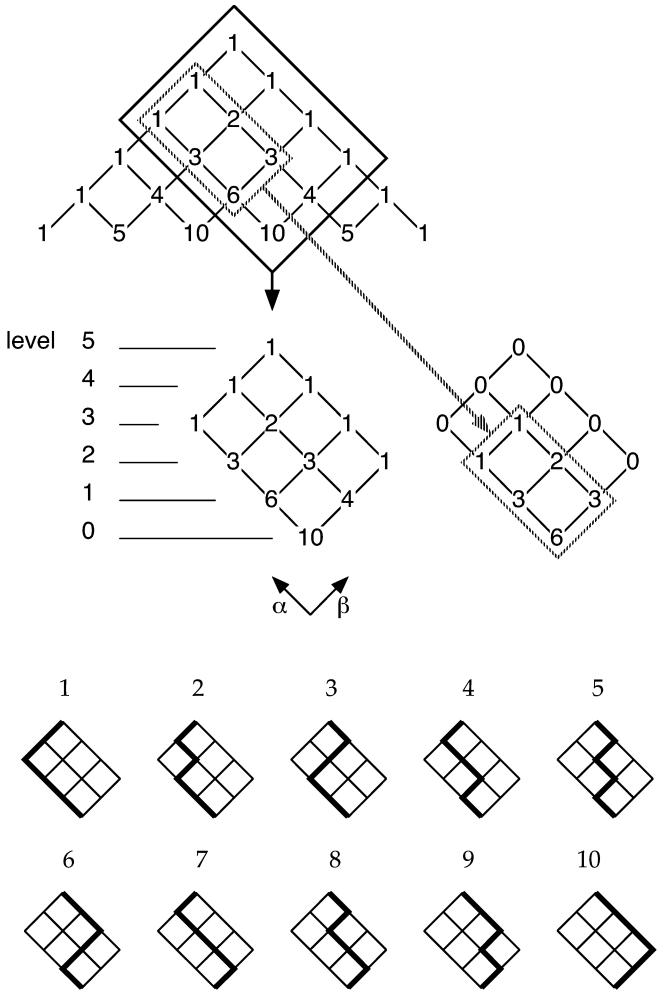

Fig. 5. Using Pascal's triangle to generate basis functions for a five-electron Heisenberg Hamiltonian (c.f. Fig. 1)

The new direct matrix element code was tested against one which reads a file of symbolic matrix elements produced elsewhere [27], filtered to give matrix elements between perfect-pairing VB basis functions only. Both Slater determinant and spin-adapted CSF bases were generated this way, checking that they gave the same energies for the appropriate states.

As a further test, we checked the symmetry of the P_{ij} "spin exchange" density matrix [11,30]:

$$P_{ij} = \sum_{KL} C_K C_L \Gamma_{ij}^{KL} \quad -1 \le P_{ij} \le 1$$

Here, C_K is the expansion coefficient of basis function K for a particular state, i and j are active orbitals and Γ_{ij}^{KL} are spin-coupling coefficients (± 1 for the Slater determinant basis). The nonzero spin-coupling coefficients are determined to within a sign by the graphical method described in the Theory section. If the molecule has, for example, D_{3h} symmetry (phenalenyl D_0), does the P_{ij}? The P_{ij} matrix has also proved very useful in the past because it can be used to label a particular "electronic isomer", and thus characterise a state regardless of whether it is for example D_0 or D_1 at a particular geometry [30]. Furthermore, the P_{ij} are related to the total spin [28,29] by

$$\langle S^2 \rangle = \frac{-N(N-4)}{4} - \sum_{ij} P_{ij} \ ,$$

where N is the number of electrons.

The next tests used MMVB to evaluate Q_{ij} and K_{ij}. MMVB [12] is a hybrid QM/MM method, which uses the MM2 potential [31] to describe the inert σ-bonded molecular framework. The active electrons – those involved in conjugation or new σ-bond formation – are represented by a Heisenberg Hamiltonian [10,32] in the space of neutral VB configurations. Because of this, the MMVB method can only treat covalent states at present, and the active sites are currently only parameterised for sp^2/sp^3 carbon atoms.

Using effective Hamiltonian theory, a CASSCF wave function with localised active orbitals can be projected onto the space of neutral valence-only VB structures [10], and interpreted as a Heisenberg Hamiltonian [9,26,32]. Heisenberg-like VB Hamiltonians are particularly suitable for parameterisation, because of the distance and orientation dependence of their matrix elements Q_{ij} and K_{ij} (like those in the Heitler–London VB treatment of the H_2 molecule [33,34]) which leads to formulae which are evaluated analytically in MMVB [12].

Finally, MMVB energies and geometries were compared with the results of ab initio calculations. For CASSCF calculations, we used MOLPRO [35] for phenalenyl to take advantage of D_{3h}/C_{2v} point group symmetry. CASSCF calculations were run using the 4-31G basis set, as this was the one used to parameterise MMVB originally. TDDFT [36] calculations were run with Gaussian [27], using the hybrid B3LYP functional and the 6-31G* basis set.

4 Results

4.1 Cyclopentadienyl

The cyclopentadienyl radical is an example of a conical intersection enforced by symmetry: a Jahn–Teller crossing [37,38,39]. The degenerate $^2E_1''$ ground state at D_{5h} geometries distorts to give the alternating C_{2v} minima (M) ($^2B_2$ electronically) and saddle points (TS) ($^2A_2$) illustrated in Fig. 6 [40].

Cyclopentadienyl has been extensively studied experimentally by Yu and coworkers [14,41,42,43] and others [44] over the last decade. We have previously [45] calculated the critical points on the D_0 and D_1 potential-energy surfaces shown in Fig. 6 using CASSCF/cc-pVDZ. We also briefly discussed the problems which

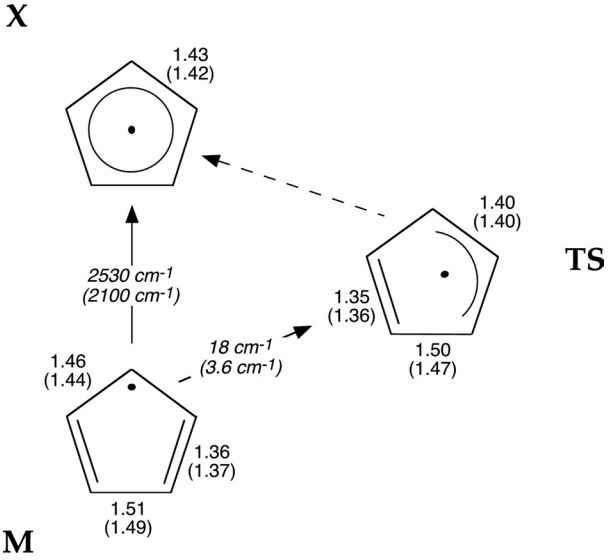

Fig. 6. Cyclopentadienyl: molecular mechanics VB (MMVB)-optimised minima (M), transition structures (TS) and Jahn–Teller crossing (X) on the D_0 and D_1 potential energy surfaces. Bond lengths in angstroms; energy differences in reciprocal centimetres (CASSCF/cc-pVDZ values in parentheses, taken from Ref. [45].)

arise [46] in trying to compare these geometries directly to those obtained from experiment.

The cyclopentadienyl structures optimised with MMVB are also shown in Fig. 6. MMVB reproduces the CASSCF bond lengths (in parentheses) to within ±2%. The larger errors are for bond lengths around 1.5Å, which are weakly π-bonded and appear to be less well described by the parameterised VB calculation. One bond length can be checked directly against experiment: for the D_{5h} Jahn–Teller crossing X, a C–C bond length of 1.421Å was determined by Yu et al. [14]. Both MMVB and CASSCF [45] reproduce this well.

We now discuss the relative energies of M, TS and X. Early electron spin resonance spectra at 120 K suggested that the spin distribution around the cyclopentadienyl ring was uniform [47, 48], implying that the barrier height for pseudorotation [49] between the five equivalent minima was of the order of reciprocal centimetres, resulting in a time-averaged D_{5h} structure. The MMVB (18 cm^{-1}) and CASSCF (3.6 cm^{-1}) results for the M→TS ← M barrier are both consistent with this, and both methods predict that the dienylic structure is the D_0 minimum M in agreement with previous calculations [50,51]. The energy barrier around the "moat" [37] is much smaller than the stabilisation energy due to the static Jahn–Teller distortion from the D_{5h} geometry X, which is 2530 cm^{-1} with MMVB and 2100 cm^{-1} with CASSCF.

Energy and gradient calculations with MMVB are many orders of magnitude faster than with CASSCF, making direct dynamics simulations (avoiding prior fitting of a potential energy surface [52,53]) feasible [54]. The main reason for studying cyclopentadienyl with MMVB is to be able to investigate the dynamics of a Jahn–Teller system this way. Given the differences in energetics between MMVB and CASSCF described previously, it may be that the current MMVB parameterisation is not accurate enough for dynamics; however, it is now possible to refine this parameterisation for a particular molecule [55], a procedure that was successfully used to model the photochemical decay pathways of *cis*-butadiene with direct dynamics [56].

4.2 Phenalenyl

Highly resolved excitation and emission spectra of phenalenyl in *n*-pentane at 20 K were reported in 1984 [15]. The crystal structure of the 2,5,8-tri-*tert*-butyl phenalenyl radical was recently obtained [57], in which the molecule forms a π-dimeric pair (3.3 Å separation) with a staggered arrangement of *tert*-butyl groups avoiding steric repulsion. Ab initio calculations were used [58] to investigate the strong antiferromagnetic coupling of the dimeric pair [59,60], but no geometry optimisations were carried out [61].[1] Interest in phenalenyl has recently increased further with the characterisation of a spiro-biphenalenyl radical as a prototype neutral radical molecular conductor [16] which has now been shown to be electrically, optically, and magnetically bistable [62,63].

Phenalenyl is an odd alternant radical [64] with 13 π electrons. Fig. 7 shows that MMVB and CASSCF/4-31G both predict it to have the same D_{3h} ground-state structure, with bond lengths varying from 1.40 to 1.43 Å. The bond lengths predicted by MMVB and CASSCF agree to within ±0.01 Å, and are within ±0.005 Å of those calculated with B3LYP/6-31G* (not shown). This agreement between a range of theoretical methods suggests that the bond lengths we calculate are reliable. However, the bond alternation calculated for D_0 phenalenyl is less than that of 1.37–1.42 Å predicted from the crystal structure of the π dimer [57], which was compared to the alternation found in naphthalene. We also found this wider range of bond lengths in naphthalene with MMVB [11] in agreement with previous CASSCF calculations [65]. However, for the isolated phenalenyl radical, our calculations appear to show that the three rings of phenalenyl are more benzene-like in the ground state than the two rings in naphthalene.

MMVB and CASSCF also predict very similar values for the vertical excitation energies of phenalenyl: 57.6 and 61.7 kcal mol^{-1}, respectively. (The corresponding TDDFT value, using B3LYP/6-31G*, is 63.7 kcal mol^{-1}). As suggested by Cofino et al. [15], the first excited state with the same spin multiplicity as the ground state is a degenerate Jahn–Teller pair. With MMVB, these are not the first excited states: we also find a state with spin multiplicity 3.75 (three unpaired spins), 4.4 kcal mol^{-1} below the degenerate pair.[2]

Fig. 7 also shows the minima M, D_1, and transition structures TS, D_1 which surround the excited-state Jahn–Teller crossing. With CASSCF, it was straightforward to optimise these structures – which both have C_{2v} symmetry – by constraining the wavefunctions to have either A_2 or B_2 symmetry. With MMVB, this was not possible, and the existence of the state with three unpaired spins presented an additional problem. The solution was to look at the spin density matrix P_{ij} computed near the D_{3h} vertically excited geometry for the two states of the Jahn–Teller pair, to determine whether the π bonds would extend or contract on relaxation away from the degeneracy. Different distortions were determined for each state, and a small initial displacement in the appropriate direction meant that M, D_1 or TS, D_1 could be optimised on the first excited state. The resulting MMVB geometries agree fairly well with those obtained with CASSCF, although a number of bond lengths are outside the ±0.01 Å tolerance.

With optimised excited-state geometries M, D_1 and TS, D_1, several relative energies can be compared between MMVB and CASSCF, and there is good agreement for each. Fig. 7 shows that the relaxation energies from the D_{3h} D_0* geometry to the C_{2v} minima and TS are comparable, with the MMVB values being larger. MMVB also overestimates the barrier to "pseudorotation" around the Jahn–Teller moat (further illustrated

[1] There are DFT calculations of the electron affinity of perinaphthenyl = phenalenyl, but no optimised geometries were reported.

[2] The same pattern of states/spin multiplicities is also obtained with Huckel-like parameters (1.0 coupling between adjacent spin sites) in the standalone Heisenberg Hamiltonian calculation, which with 1716 determinant basis functions is currently near the limit for tests involving full diagonalisation of the Hamiltonian.

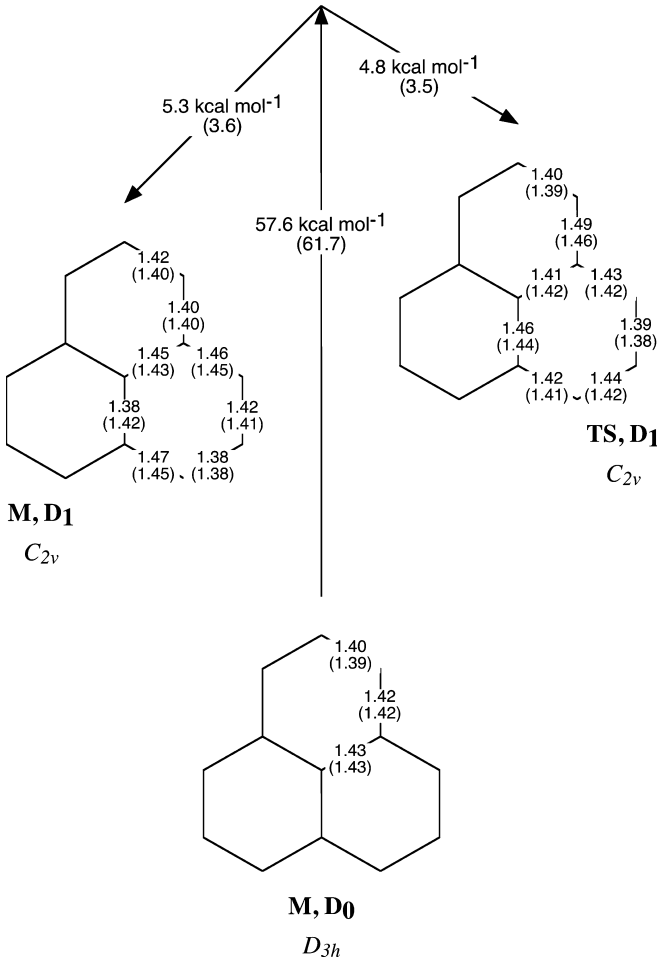

Fig. 7. Phenalenyl: MMVB-optimised structures on the D_0 and D_1 potential energy surfaces. Bond lengths in angstroms (only unique bond lengths are shown); energy differences in kilocalories per mole. CASSCF/4-31G values in parentheses

in the supplementary material), with a value of 0.5 kcal mol^{-1} to compare with 0.1 kcal mol^{-1} for CASSCF. Finally, the 0-0 transition was found to be 18679 $cm^{-1} = 53.4$ kcal mol^{-1} from high-resolution laser spectroscopy [15]; MMVB predicts 52.3 kcal mol^{-1} and CASSCF 58.1 kcal mol^{-1}. This agreement is perhaps surprising because of the small one-electron basis set (4-31G) used; however, we have previously shown that for planar geometries [11,66] of the valence excited states for which MMVB is valid, large basis sets are not always necessary [67]. MMVB was originally parameterised from 4-31G CASSCF calculations, which is why 4-31G was used for the CASSCF calculations described here.

In summary: The MMVB, CASSCF, and TDDFT results are in good agreement for phenalenyl, and the predicted excitation energies are comparable with experiment. These are the first ab initio calculations on the excited states of phenalenyl.

4.3 Triphenylmethyl

The triphenylmethyl radical was originally characterised by Gomberg [18]. Experimentally, the D_0-D_1 absorption is weak [13] but is detected at 440 nm [17]; λ_{max} is at 337 nm. Temperature-dependent fluorescence is detected at 520 nm [68], $E_a = 4.6$ kcal mol^{-1}. Solution excitation at room temperature does not give emission on the nanosecond timescale [68,69,70]. Instead, a ring-closure reaction pathway opens up, as shown in Scheme 1 [17]. The resulting DHPM radical is detected within 10 ns, has a 100-μs lifetime, and absorbs at 490 nm [71].

Triphenylmethyl is a 19-electron π system, which is nonplanar because of steric repulsion between the three benzene rings. It was chosen as a test case here because it is a radical with a barrier-activated channel for radiationless excited-state decay, leading to a chemical reaction (ring closure [17,71]). MMVB can describe the formation of new σ bonds from p orbitals in a π system. However, we encountered some problems here with the parameterisation of the terms in the Heisenberg Hamiltonian needed to describe this new bond formation: specifically, the behaviour of the formulae for determining Q_{ij} at long range (beyond 2.5 Å), which do not tend to zero smoothly. To try to minimise the problem, we included only the Q_{ij} terms necessary to describe the formation of the one new σ bond (Scheme 1). The compromise here is that the D_0 minimum of triphenylmethyl (Fig. 8) no longer has the correct D_3 point group symmetry because of the unsymmetric potential, and we must use the same potential throughout for consistent energetics. Reassuringly, when the extra term in the MMVB potential is removed, M_{open}, D_0 has the correct D_3 symmetry, and the bond lengths are all within ± 0.01 Å of the B3LYP/6-31G* (Fig. 9) values. The remaining critical points (Fig. 8) only have C_2 symmetry, so the problem is not as obvious. Calibration against CASSCF calculations is unfortunately not possible at present for triphenylmethyl because the necessary active space is too large, so we cannot estimate what effect the problems in the MMVB potential have on the relative energetics.

Fig. 8 shows critical points located with MMVB on the D_0 and D_1 potential energy surfaces of triphenylmethyl. There are closed and open minima on both surfaces, and a D_1/D_0 conical intersection [72,73] that is midway between the two. For the open form, the D_1 excitation is strongly localised in two of the benzene rings, reminiscent of one of the excited-state structures previously located with MMVB for *cis*-stilbene [74]. The triphenylmethyl conical intersection is also similar to the "cooperating rings" crossing located in *cis*-stilbene: here, one ring is a passive spectator and a new bond is formed between the other two, which now have localised single and double bonds.

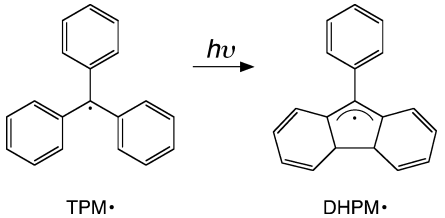

Scheme 1.

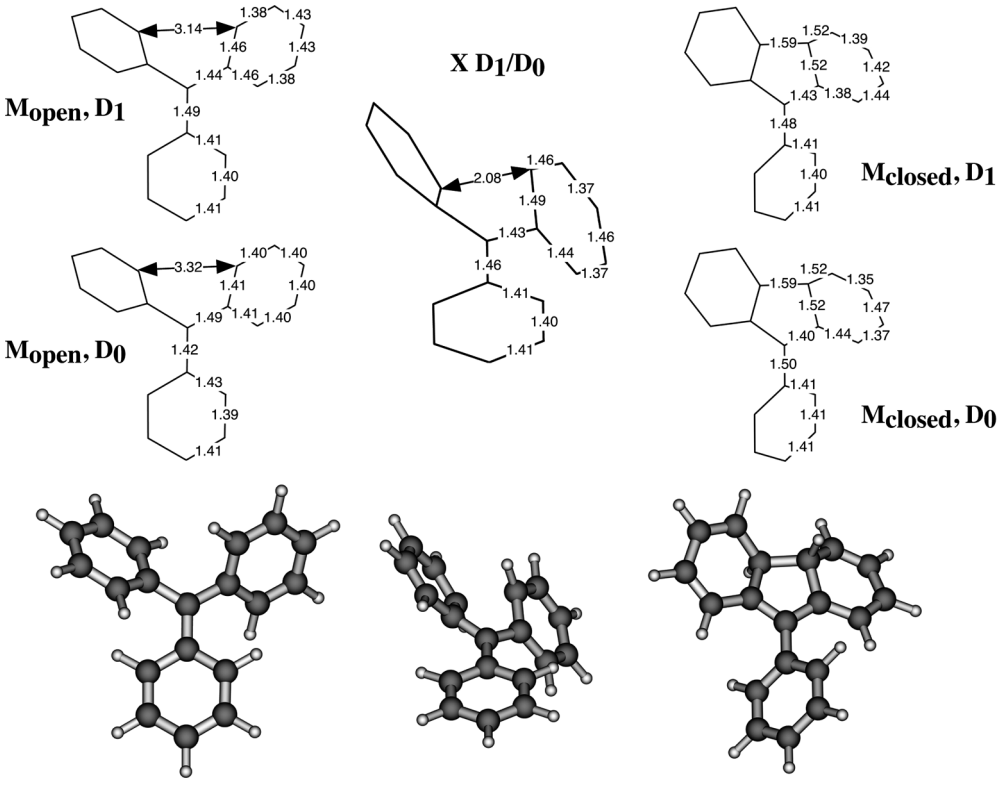

Fig. 8. Triphenylmethyl: MMVB-optimised structures on the D_0 and D_1 potential energy surfaces. Bond lengths in angstroms. Only unique bond lengths are shown, as all structures have a C_2 symmetry axis. (M_{closed}, D_0 does not have the expected C_3 symmetry because of a long-range defect in the MMVB parameters necessary to describe the formation of the new σ bond, as discussed in the text)

The relative energetics of the critical points shown in Fig. 8 are indicated in Fig. 10. This figure is derived from linear interpolations on the D_0 and D_1 potential energy surfaces. This will give upper bounds to any energy barriers between points, although it is approximate, and it is important to note that the interpolation coordinates used on D_0 and D_1 are different.

Several energy differences from Fig. 10 can be compared with experiment. The barrier from M_{open}, D_1 to the crossing X D_1/D_0 is calculated to be 14 kcal mol^{-1}. This is larger than the experimentally-estimated barrier for the radiationless channel leading from open to closed forms of 4.6 kcal mol^{-1}. Secondly, we can identify the 520 nm ($\sim$55 kcal mol^{-1}) fluorescence of the open form with the energy difference between M_{open}, D_1 and M_{open}, D_0. With MMVB, we calculate this value to be 44 kcal mol^{-1}, regardless of whether the potential includes the term necessary to describe the new σ bond. Finally, if the 440 nm (around 65 kcal mol^{-1}) absorption of triphenylmethyl corresponds to the vertical excitation to D_1, MMVB underestimates this by 19 kcal mol^{-1}. Although there are known problems with determining vertical excitation energies, a TDDFT (B3LYP/6-31G*) calculation at the M_{open}, D_0 geometry shown in Fig. 9 predicts a vertical excitation energy to D_1 (low intensity, $f = 0.0087$) of 67 kcal mol^{-1}, which is close to the experimental value. If we have identified the transitions correctly, MMVB does not appear to describe the energy differences in the nonplanar triphenylmethyl as well as in the planar cyclopentadienyl and phenalenyl radicals.

In summary: We have located a reaction path from the excited-state open form of triphenylmethyl to the closed form directly via a conical intersection, which is consistent with the observed barrier-activated radiationless decay. However, we are not yet certain that this is the reactive state, because of problems with the MMVB potential, and there is a chance that we are calculating "dark" states which are not observed spectroscopically.

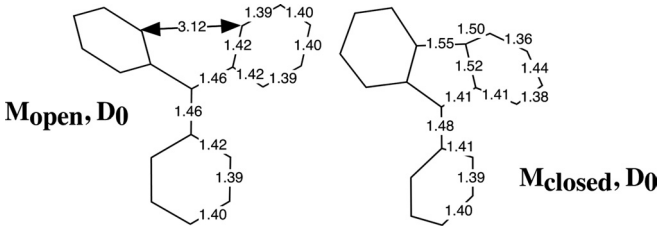

Fig. 9. Triphenylmethyl: open and closed minima on D_0 optimised with B3LYP/6-31G*. Bond lengths in angstroms

5 Conclusion

A pictorial method for generating Heisenberg Hamiltonian matrix elements was described, reviewing [11]. The code is basically in three parts:

1. Generate n and $n-2$ grids based on Pascal's triangle.
2. Generate all possible n walks $\Rightarrow$ diagonal matrix elements.
3. Generate all possible $n-2$ walks $\Rightarrow$ offdiagonal matrix elements for the n problem.

There are many other codes for generating such matrix elements [9,22,23,24,25,26]. Part of the reason for

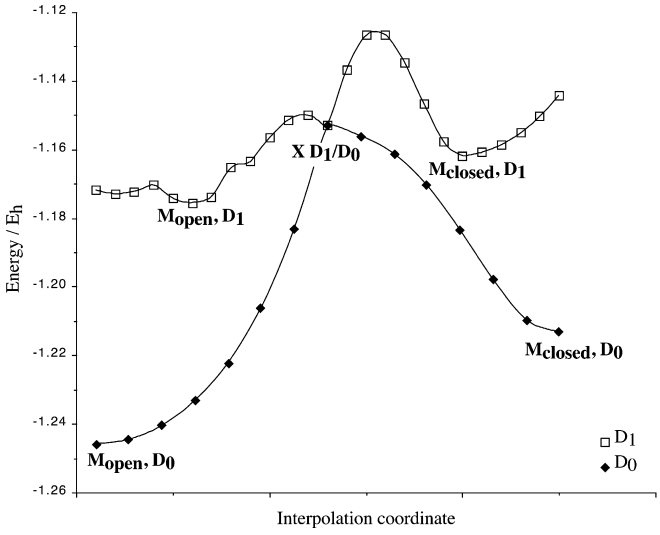

Fig. 10. Triphenylmethyl: linear interpolations from the X D_1/D_0 conical intersection to the closed and open minima on the D_1 and D_0 potential energy surfaces. The crossing X and four minima M (shown in Fig. 8) were fully optimised with MMVB

reviewing this pictorial approach is that we believe it will be straightforward to extend it to, for example, electron-transfer systems, with n electrons singly occupying $n + 1$ orbitals.

The matrix element code described here is included in the MMVB program [12]. Test calculations for odd-electron systems were carried out on the excited states of three conjugated hydrocarbon radicals: cyclopentadienyl and phenalenyl (planar); and triphenylmethyl (nonplanar). For the planar radicals, energies and geometries computed with MMVB agreed closely with those obtained with CASSCF. For triphenylmethyl, no comparison with CASSCF is currently possible. The conical intersection geometry predicted for triphenylmethyl by MMVB is consistent with the observed experimental data, explaining the barrier-activated radiationless decay. However, the energetics are marred by problems with the MMVB parameterisation.

This paper is not about parameters in the MMVB force field, but the numerical values of Q_{ij} and K_{ij} have to be obtained somehow, and practical applications are at present mainly limited by the quality of these parameters. Some progress on improving these has recently been made [55].

Acknowledgements. Based on work supported by DuPont. All code development and MMVB calculations were carried out on an Apple G3 PowerBook (Pismo) running Yellow Dog Linux 2.0. Some images were produced using Molden [75]. Many thanks to M. A. Robb for comments on the manuscript and for suggesting a graphical approach to this problem originally, and Marc Zeedar for Z-Write.

References

1. Robb MA (2000) Theor Chem Acc 103: 317
2. Paldus J (1974) J Chem Phys 61: 5321
3. Robb MA, Niazi U (1984) Comput Phys Rep 1: 127
4. Robb MA, Niazi U (1990) Rep Mol Theor 1: 23
5. Shavitt I (1977) Int J Quantum Chem Symp 11: 131
6. Shavitt I (1978) Int J Quantum Chem Symp 12: 5
7. Shavitt I (1998) Mol Phys 94: 3
8. Duch W (1991) J Mol Struct (THEOCHEM) 234: 27
9. Said M, Maynau D, Malrieu JP, Bach MAG (1984) J Am Chem Soc 106: 571
10. Bernardi F, Olivucci M, McDouall JJW, Robb MA (1988) J Chem Phys 89: 6365
11. Bearpark MJ, Robb MA, Bernardi F, Olivucci M (1994) Chem Phys Lett 217: 513
12. Bernardi F, Olivucci M, Robb MA (1992) J Am Chem Soc 114: 1606
13. Johnston LJ (1993) Chem Rev 93: 251
14. Yu L, Cullin DW, Williamson JM, Miller TA (1993) J Chem Phys 98: 2682
15. Cofino WP, van Dam SM, Kamminga DA, Hoornweg GPh, Gooijer C, Maclean C, Velthorst NH (1984) Mol Phys 51: 537
16. Chi X, Itkis ME, Patrick BO, Barclay TM, Reed RW, Oakley RT, Cordes AW, Haddon RC (1999) J Am Chem Soc 121: 10395
17. Schmidt JA, Hilinski EF (1988) J Am Chem Soc 110: 4036
18. Gomberg M (1900) J Am Chem Soc 12: 757
19. Kline M (1990) Mathematical thought from ancient to modern times, vol 1. Oxford University Press, Oxford, p 272
20. Knowles PJ, Handy NC (1984) Chem Phys Lett 111: 315
21. Alexander SA, Schmalz TG (1987) J Am Chem Soc 109: 6933
22. Flocke N, Karwowski J (1997) Phys Rev B 55: 8287
23. Flocke N, Schmalz TG (1998) Chem Phys Lett 298: 71
24. Li S, Ma J, Jiang Y (1996) J Phys Chem 100: 4775
25. Sarma CR, Ghosh DK, Kadolkar CY (1999) Int J Quantum Chem 73: 389
26. Maynau D, Durand P, Daudey JP, Malrieu JP (1983) Phys Rev A 28: 3193
27. Hegarty D, Robb MA (1979) Mol Phys 38:1795, implemented in Frisch MJ, Trucks GW, Schlegel HB, Scuseria GE, Robb MA, Cheeseman JR, Zakrzewski VG, Montgomery JA, Jr, Kudin KN, Burant JC, Millam JM, Stratmann RE, Tomasi J, Barone V, Mennucci B, Cossi M, Scalmani G, Rega N, Iyengar S, Petersson GA, Ehara M, Toyota K, Nakatsuji H, Adamo C, Jaramillo J, Cammi R, Pomelli C, Ochterski J, Ayala PY, Morokuma K, Salvador P, Dannenberg JJ, Dapprich S, Daniels AD, Strain MC, Farkas O, Malick DK, Rabuck AD, Raghavachari K, Foresman JB, Ortiz JV, Cui Q, Baboul AG, Clifford S, Cioslowski J, Stefanov BB, Liu G, Liashenko A, Piskorz P, Komaromi I, Gomperts R, Martin RL, Fox DJ, Keith T, Al-Laham MA, Peng CY, Nanayakkara A, Challacombe M, Gill PMW, Johnson B, Chen W, Wong MW, Andres JL, Gonzalez C, Head-Gordon M, Replogle ES, Pople JA (2001) Gaussian 01, development version (B.01), Gaussian, Pittsburgh, PA
28. Dirac PAM (1929) Proc R Soc Lond Ser A 123: 714
29. Kutzelnigg W (2000) Theor Chem Acc 103: 182
30. Celani P, Blancafort L, Bearpark MJ, Robb MA (2003) Theor Chem Acc (accepted)
31. Allinger NL (1976) Adv Phys Org Chem 13: 1
32. Durand P, Malrieu JP (1987) Adv Chem Phys 67: 321
33. Heitler W, London F (1927) Z Phys 44: 455
34. Frenking G (2000) Theor Chem Acc 103: 177
35. Werner H-J, Knowles PJ, Amos RD, Bernhardsson A, Berning A, Celani P, Cooper DL, Deegan MJO, Dobbyn AJ, Eckert F, Hampel C, Hetzer G, Korona T, Lindh R, Lloyd AW, McNicholas SJ, Manby FR, Meyer W, Mura ME, Nicklass A, Palmieri P, Pitzer R, Rauhut G, Schütz M, Schumann U, Stoll H, Stone AJ, Tarroni R, Thorsteinsson T MOLPRO
36. Casida ME, Jamorski C, Casida KC, Salahub DR (1998) J Chem Phys 108: 4439
37. Herzberg G (1966) Electronic spectra of polyatomic molecules. Van Nostrand, New York, pp 48, 443
38. Jahn HA, Teller E (1936) Phys Rev 49: 874
39. Jahn HA, Teller E (1937) Proc R Soc and Ser A 161: 220
40. Salem L (1966) The molecular orbital theory of conjugated systems. Benjamin, New York, p 470

41. Yu L, Foster SC, Williamson JM, Heaven MC, Miller TA (1988) J Phys Chem 92: 4263
42. Yu L, Williamson JM, Miller TA (1989) Chem Phys Lett 162: 431
43. Cullin DW, Yu L, Williamson JM, Miller TA (1992) J Phys Chem 96: 89
44. Ihee H, Feenstra JS, Cao J, Zewail AH (2002) Chem Phys Lett 353: 325
45. Bearpark MJ, Robb MA, Yamamoto N (1999) Spectrochim Acta Part A 55: 639
46. Applegate BE, Miller TA, Barckholz TA (2001) J Chem Phys 114: 4855
47. Onishi SI, Itta I (1963) J Chem Phys 39: 2848
48. Liebling GR, McConnell HM (1965) J Chem Phys 42: 3931
49. Liehr AD (1963) J Phys Chem 67: 389
50. Meyer R, Graf F, Ha T-K, Günthard HH (1979) Chem Phys Lett 66: 65
51. Borden WT, Davidson ER (1979) J Am Chem Soc 101: 3771
52. Helgaker T, Uggerud E, Jensen HJA (1990) Chem Phys Lett 173: 145
53. Chen W, Hase WL, Schlegel HB (1994) Chem Phys Lett 228: 436
54. Bearpark MJ, Bernardi F, Clifford S, Olivucci M, Robb MA, Smith BR, Vreven T (1996) J Am Chem Soc 118: 169
55. Garavelli M, Ruggeri F, Ogliaro F, Bearpark MJ, Bernardi F, Olivucci M, Robb MA (2003) J Comput Chem 24: 1357
56. Garavelli M, Bernardi F, Olivucci M, Bearpark MJ, Klein S, Robb MA (2001) J Phys Chem A 105: 11496
57. Goto K, Kubo T, Yamamoto K, Nakasuji K, Sato K, Shiomi D, Takui T, Kubota M, Kobayashi T, Yakusi K, Ouyang J (1999) J Am Chem Soc 121: 1619
58. Takano Y, Taniguchi T, Isobe H, Kubo T, Morita Y, Yamamoto K, Nakasuji K, Takui T, Yamaguchi K (2002) Chem Phys Lett 358: 17
59. Fukui K, Sato K, Shiomi D, Takui T, Itoh K, Gotoh K, Kubo T, Yamamoto K, Nakasuji K, Naito A (1999) Synth Met 103: 2257
60. Fukui K, Sato K, Shiomi D, Takui T, Itoh K, Kubo T, Gotoh K, Yamamoto K, Nakasuji K, Naito A (1999) Mol Cryst Liq Cryst 334: 49
61. Rienstra-Kiracofe JC, Barden CJ, Brown ST, Schaefer HF (2001) J Phys Chem A 105: 524
62. Chi X, Itkis ME, Kirschbaum K, Pinkerton AA, Oakley RT, Cordes AW, Haddon RC (2001) J Am Chem Soc 123: 4041
63. Itkis ME, Chi X, Cordes AW, Haddon RC (2002) Science 296: 1443
64. Clar E (1972) The aromatic sextet. Wiley, London, pp 107–113
65. Swiderek P, Hohlneicher G, Maluendes SA, Dupuis M (1993) J Chem Phys 98: 975
66. Bearpark MJ, Bernardi F, Olivucci M, Robb MA (1997) J Phys Chem A 101: 8395
67. Matos JMO, Roos BO, Malmqvist PA (1987) J Chem Phys 86:1458
68. Bromberg A, Schmidt KH, Meisel D (1984) J Am Chem Soc 106: 3056
69. Bromberg A, Schmidt KH, Meisel D (1985) J Am Chem Soc 107: 83
70. Meisel D, Das PK, Hug GL, Bhattacharyya K, Fessenden RW (1986) J Am Chem Soc 108: 4706
71. Siskos MG, Zarkadis AK, Steenken S, Karakostas N, Garas SK (1998) J Org Chem 63: 3251
72. Yarkony DR (1998) Acc Chem Res 31: 511
73. Bearpark MJ, Robb MA, Schlegel HB (1994) 223: 269
74. Bearpark MJ, Bernardi F, Clifford S, Olivucci M, Robb MA, Vreven T (1997) J Phys Chem A 101: 3841
75. Schaftenaar G, Noordik JH (2000) J Comput-Aided Mol Des 14: 123–134